

# Water entry of spheres with various contact angles

Nathan B. Speirs<sup>1</sup>, Mohammad M. Mansoor<sup>1</sup>, Jesse Belden<sup>2</sup>  
and Tadd T. Truscott<sup>1,†</sup>

<sup>1</sup>Department of Mechanical and Aerospace Engineering, Utah State University, Logan, UT 84322, USA

<sup>2</sup>Naval Undersea Warfare Center, 1176 Howell Street, Newport, RI 02841, USA

(Received 5 September 2018; revised 19 November 2018; accepted 4 December 2018; first published online 10 January 2019)

It is well known that the water entry of a sphere causes cavity formation above a critical impact velocity as a function of the solid–liquid contact angle; Duez *et al.* (*Nat. Phys.*, vol. 3 (3), 2007, pp. 180–183). Using a rough sphere with a contact angle of 120°, Aristoff & Bush (*J. Fluid Mech.*, vol. 619, 2009, pp. 45–78) showed that there are four different cavity shapes dependent on the Bond and Weber numbers (i.e., quasistatic, shallow, deep and surface). We experimentally alter the Bond number, Weber number and contact angle of smooth spheres and find two key additions to the literature: (1) cavity shape also depends on the contact angle; (2) the absence of a splash crown at low Weber number results in cavity formation below the predicted critical velocity. In addition, we use alternate scales in defining the Bond, Weber and Froude numbers to predict the cavity shapes and scale pinch-off times for various impacting bodies (e.g., spheres, multidroplet streams and jets) on the same plots, merging the often separated studies of solid–liquid and liquid–liquid impact in the literature.

**Key words:** interfacial flows (free surface)

## 1. Introduction

At the turn of the millennium a resurgence of interest occurred in water entry studies. During this time, two foundational papers on cavity formation and cavity dynamics were published, which describe the regimes into which all other water entry studies fall. The first was written by Duez *et al.* (2007), who greatly expanded the previous work of May (1951) explaining when impacting spheres form air cavities, as shown in figure 1(*b–e*), and when they do not, as shown in figure 1(*a*). The second paper, written by Aristoff & Bush (2009), came along a couple of years later,

<sup>†</sup> Email address for correspondence: [taddtruscott@gmail.com](mailto:taddtruscott@gmail.com)

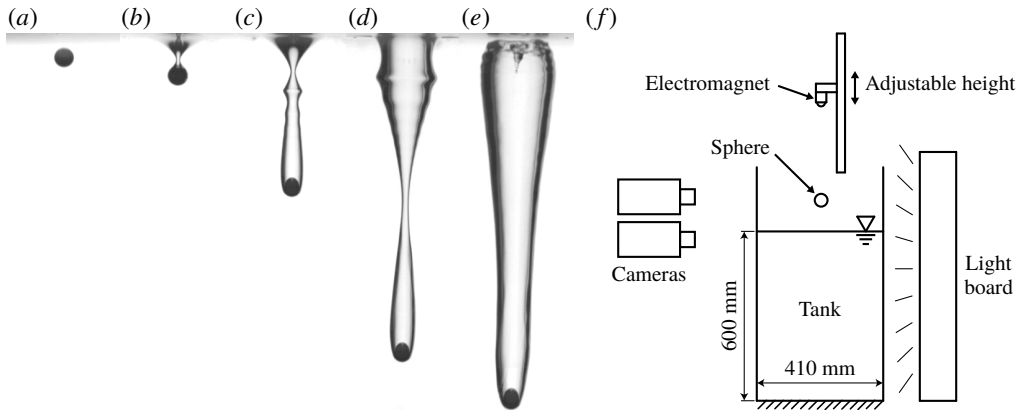


FIGURE 1. A 2 mm diameter sphere impacts the water surface creating various cavity types. In (a) the wetting angle is  $\theta = 101^\circ$  and the sphere impacts at  $4.43 \text{ m s}^{-1}$  without forming a cavity. In (b–e) the sphere has a wetting angle of  $\theta = 141^\circ$  and impacts with velocities  $0.24 \text{ m s}^{-1}$ ,  $1.40 \text{ m s}^{-1}$ ,  $2.80 \text{ m s}^{-1}$  and  $4.43 \text{ m s}^{-1}$ , forming quasistatic, shallow, deep and surface seal cavities, respectively. See supplementary movies 1–5 (available at <https://doi.org/10.1017/jfm.2018.985>). (f) The basic experimental set-up is shown with two high-speed cameras viewing the impact events above and below the free surface.

discussing the four different shapes or types of cavity that form once the appropriate conditions are met for cavity formation (shown in figure 1b–e). We will now examine each of these papers in turn, discussing their findings, an unaddressed discrepancy between the two, and how this paper expands our understanding of the conditions in which these five water entry regimes occur.

Duez *et al.* (2007) found that cavity formation of smooth spheres occurs above a critical velocity  $U_{cr}$  that is a function of the advancing static contact angle  $\theta$ . Hydrophilic spheres ( $\theta < 90^\circ$ ) form cavities above  $U_{cr} \approx 7.2 \text{ m s}^{-1}$  in water. The critical velocity decreases for hydrophobic spheres ( $\theta > 90^\circ$ ), going to zero as  $\theta$  goes to  $180^\circ$ . They explain this finding by discussing the contact-line stability of the thin, upward-moving film or splash crown that forms around the circumference of the sphere upon impact. When the splash adheres to the sphere (below the critical velocity) no cavity forms. When it separates from the sphere, air gets pulled behind the sphere and a cavity forms.

Aristoff & Bush (2009) studied the water entry of spheres with one contact angle,  $\theta = 120 \pm 5^\circ$ , and various impact velocities and sphere diameters. Their expansive data set found cavities forming at all impact velocities, with four distinct shapes defined by their collapse or pinch-off location, each of which occurs in a specific region on a Bond–Weber plot. At the lowest Weber number,  $We$ , they describe quasistatic seal, in which pinch-off occurs on or very near the sphere surface (figure 1b). At higher  $We$ , both shallow and deep seal are seen. Shallow seal occurs at lower Bond number,  $Bo$ , where surface tension dominates and the pinch-off depth is of the order of the capillary length (figure 1c). Deep seal occurs at higher  $Bo$ , where gravitational forces dominate and pinch-off occurs approximately half way between the pool surface and the sphere (figure 1d). Surface seal occurs at the highest  $We$ , wherein the splash crown created upon impact collapses inwards due to air pressure and surface tension (Marston *et al.* 2016), sealing at the pool surface (figure 1e).

According to Duez *et al.* (2007), at the contact angle used by Aristoff & Bush (2009) ( $\theta = 120^\circ$ ), cavities should not form below  $U_{cr} = 2.14 \text{ m s}^{-1}$ . Yet Aristoff & Bush report quasistatic, shallow and deep seal cavities at velocities below this value. We can explain this discrepancy by the surface roughness of the coating used by Aristoff & Bush – namely Cytonix WX2100. Aristoff & Bush report a root mean squared roughness of  $R_q = 1.6 \text{ }\mu\text{m}$ . A few years later Zhao, Chen & Wang (2014) revealed that the maximum roughness  $R_z$  (defined as the sum of the highest peak and the deepest trough) predicts  $U_{cr}$  better than the root mean squared roughness. In attempting to reproduce the coating of Aristoff & Bush we obtain a coating with maximum roughness value of  $R_z = 16.9 \pm 2.4 \text{ }\mu\text{m}$ . According to Zhao *et al.* (2014) this  $R_z$  value should result in cavity formation even at very low impact velocities. Hence the cavity formation described in the work of Aristoff & Bush (2009) is due to both the high contact angle and high roughness.

Since these foundational works, several other important studies have come forth. Important topics include: the water entry of spinning spheres (Truscott & Techet 2009*a,b*), the effect of sphere density (Aristoff *et al.* 2010), the occurrence of multiple pinch-off events (Mansoor *et al.* 2014), the buckling instability in the crown (Marston *et al.* 2016), the effects of deformability (Hurd *et al.* 2017), the unsteady forces during entry (Truscott, Epps & Techet 2012), and many more described in the annual review by Truscott, Epps & Belden (2014).

Although these works have contributed much to our understanding of water entry, we will return our focus to the foundational works discussed above and examine how the cavity formation regimes respond to experimentally varying the wetting angle  $\theta$ , the sphere diameter  $d$  and the impact velocity  $U_o$ . Seeing that the sphere roughness affects the water entry behaviour in a similar manner to the contact angle (as discussed above) we restrict our study to smooth spheres with  $R_z \lesssim 1 \text{ }\mu\text{m}$ , but refer to the findings with hydrophobic and rough spheres of Aristoff & Bush (2009) for comparison. We will explain the physics using the Bond, Weber and Froude numbers, which we define as  $Bo = \rho g d^2 / \sigma$ ,  $We = \rho U_o^2 d / \sigma$  and  $Fr = U_o^2 / g d$ , respectively, where  $\rho$  is the liquid density,  $g$  is the acceleration of gravity and  $\sigma$  is the surface tension. We use the diameter  $d$  instead of the sphere radius as the appropriate length scale in defining the above dimensionless numbers, as it results in transitional behaviours around a value of one. In §4 we will also examine an alternate method of defining the Bond, Weber and Froude numbers that allows us to predict the cavity types for various impacting bodies on the same regime diagram.

## 2. Experimental set-up and description

Figure 1(*f*) shows the experimental set-up used in this study. Various diameter stainless steel spheres ( $d = 1\text{--}18 \text{ mm}$ ) of density  $7830 \text{ kg m}^{-3}$  are dropped from an electromagnet onto a tank of water. Two high-speed cameras record the impact on the free surface, imaging at 2500 frames per second both above and below the surface from the side. The height of the electromagnet controls the impact velocity of the spheres  $U_o$ , which is varied from 0.10 to  $10.39 \text{ m s}^{-1}$ . To vary the advancing static contact angle  $\theta$ , three different coatings (or the lack thereof) are used: clean steel, Turtle Wax Super Hard Shell car wax and Glaco Mirror Coat Zero. The contact angle is measured using the sessile drop method. Values of  $\theta$  and  $R_z$  are shown in table 1. Roughness measurements are obtained using a profilometer. The spheres are prepared by first washing with soap and water and then rinsing with ethyl alcohol. Coatings are then applied and allowed to dry before testing. After each test the spheres are dried and then recoated to ensure consistent surface properties.

Coating	$\theta$	$R_z$ ( $\mu\text{m}$ )
Clean steel	$86 \pm 2^\circ$	$0.6 \pm 0.3$
Turtle wax super hard shell	$101 \pm 5^\circ$	$0.9 \pm 0.2$
Cytonix WX2100	$117 \pm 7^\circ$	$16.9 \pm 2.4$
Glaco mirror coat zero	$141 \pm 4^\circ$	$1.0 \pm 0.5$

TABLE 1. List of coatings with their advancing static contact angle  $\theta$  and maximum roughness  $R_z$ , with the mean and 95% confidence window reported.

From the high-speed videos we determine whether or not a cavity forms. If a cavity does form, the cavity type is determined using the definitions described by Aristoff & Bush (2009). Measurements are also taken from the videos to find cavity depths, diameters and the time to pinch-off. The pinch-off depth  $h_p$  is defined as the distance from the undisturbed free surface to the location where the cavity walls or splash crown pinch together or collapse (positive downward). The depth of the bottom of the sphere at the time of pinch-off,  $h_b$ , is also measured from the undisturbed free surface. The pinch-off time  $t_p$  is defined as the time from impact to the pinch-off event. In cases where cavities do not form, we define the pinch-off time  $t_p$  as the time when the splash crown closes on the top of the sphere and the pinch-off depth  $h_p$  as the location of the top of the sphere at this time. The cavity diameter is measured at discrete depths (each row of pixels) and times (each frame) and the maximum cavity diameter from impact to the time of pinch-off is found at each discrete depth, yielding  $d_{c,max}(z)$ . The average of these maximum diameters over all depths defines  $d_c$  (further explanation of this same method for calculating  $d_c$  can be found in Speirs *et al.* (2018)).

### 3. Cavity formation and types for different contact angles

Multiple sphere diameters were tested over a large range of impact velocities for each contact angle. From these data we produce *Bo-We* plots similar to Aristoff & Bush (2009) to examine how the cavity regimes change with the contact angle (figure 2). The regime diagram for  $\theta = 86^\circ$  is shown in figure 2(a). Duez *et al.* (2007) predict the critical velocity for cavity formation for a hydrophilic sphere to be  $U_{cr} = 0.1\sigma/\mu = 7.2 \text{ m s}^{-1}$ , where  $\mu$  is the dynamic viscosity, which is represented by the dashed line in figure 2(a). Surface seal cavities occur above this dashed line (as shown in figure 1e) and no cavity formation is observed just below it (figure 1a). Once *We* has decreased below approximately 240, cavities start to form again, which is unexpected in light of the work of Duez *et al.* (2007). Below  $We \approx 240$ , spheres always form quasistatic seal cavities.

Looking at the regime diagram for  $\theta = 101^\circ$  (figure 2b) we see a similar trend to  $\theta = 86^\circ$  with a few differences. The critical velocity for cavity formation as predicted by Duez *et al.* (2007) has decreased due to the increased contact angle and is defined by  $U_{cr} = (7/270)(\sigma/\mu)(\pi - \theta)^3 = 4.89 \text{ m s}^{-1}$ . The critical *We* below which cavities form again does not change with the increase in  $\theta$ . Below  $We \approx 240$ , mostly quasistatic seal cavities form, with the exception of a few shallow seal cavities at low *Bo*, for which the volume of air entrained with the sphere is small, but approximately equal to the volume of the sphere (this is consistent with the cutoff defined by Aristoff & Bush (2009)).

Water entry of spheres with various contact angles

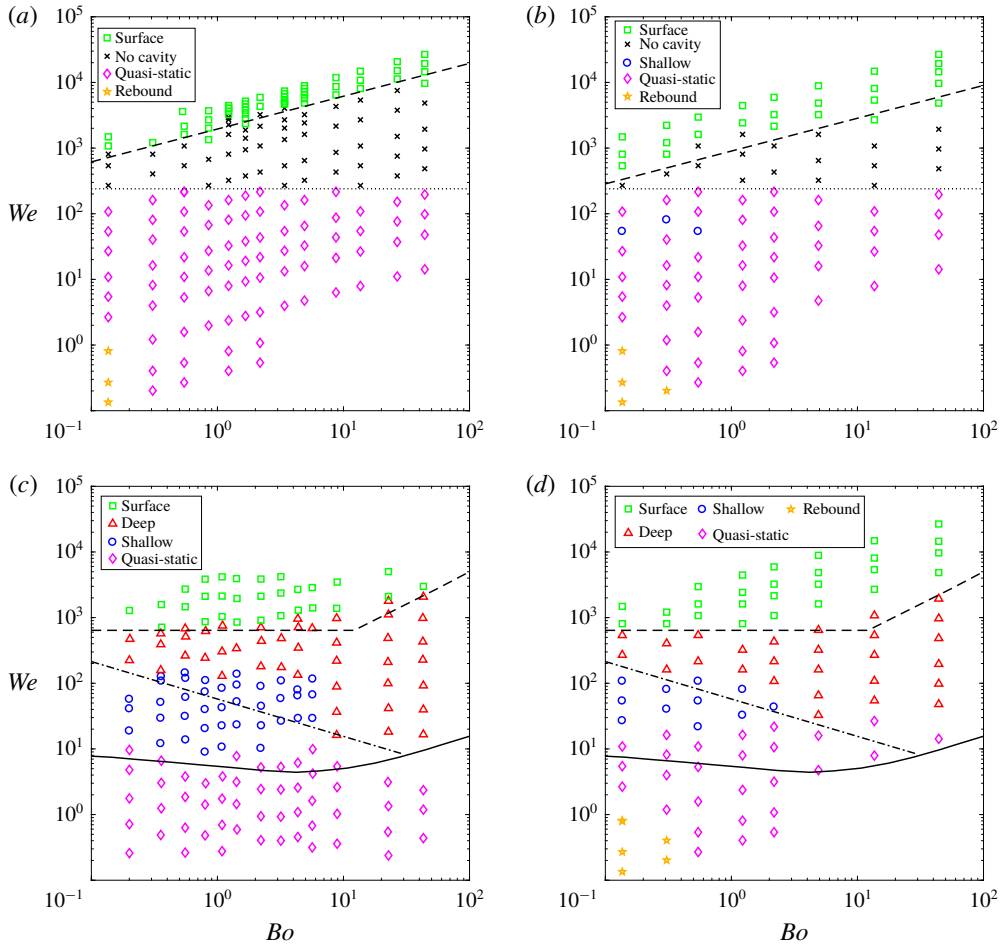


FIGURE 2. The cavity regimes for various contact angles are shown for (a)  $\theta = 86^\circ$ , (b)  $\theta = 101^\circ$ , (c)  $\theta = 120^\circ$  and  $R_z = 16.9 \mu\text{m}$  (remade from Aristoff & Bush (2009)) and (d)  $\theta = 141^\circ$ . All of the spheres ( $d = 1\text{--}18 \text{ mm}$ ) are smooth according to Zhao *et al.* (2014) except (c) (table 1). The dotted and dashed lines in (a) and (b) represent splash crown formation and Duez cavity formation, respectively. The regime separation lines in (c) and (d) are not the same as in (a) and (b). Instead they come from the predictions of Aristoff & Bush (2009). Aristoff & Bush predict the cutoffs defined by the solid curve and the dash-dotted line by equating the pinch-off times of adjacent regimes. The dashed line represents their empirical fit of  $We = 640$  for  $Bo \lesssim 10$  and for  $Bo \gtrsim 10$  it is defined by  $Fr = (1/12800)\rho^2/\rho_{air}^2$  from Birkhoff & Isaacs (1951). Pictures of the different regimes can be seen in figure 1(a–e).

To understand why cavities form below a value of  $We \approx 240$  we look at what happens as the velocity or  $We$  increases for a given sphere diameter or  $Bo$ . Figure 3(a) shows the impact of a 10 mm diameter sphere at various  $We$  when the sphere is approximately half submerged. At the lowest  $We$ , a short, thick rim forms around the edge of the sphere. This rim does not have enough upward velocity to climb up the surface of the sphere and meet itself at the pole to prevent cavity formation (Duez *et al.* 2007). Hence, as the sphere descends, the free surface is pulled down with the

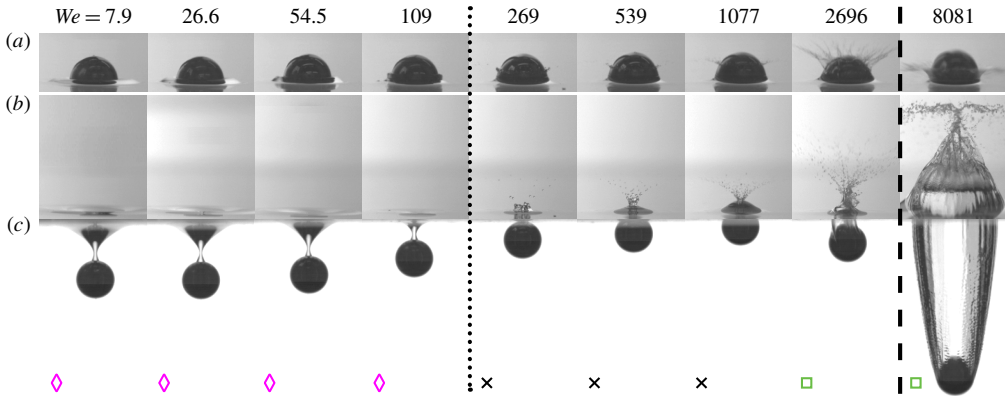


FIGURE 3. The development of the splash crown and progression of cavity regimes are shown for increasing  $We$ , for  $d = 10$  mm,  $Bo = 13.6$  and  $\theta = 101^\circ$ . Each row shows different times and/or views of the same impact event. In (a) we show the development of the rim or splash crown when the sphere is approximately half submerged. In (b,c) we show the frame just prior to pinch-off or closure of the splash crown above the sphere as viewed from above and below the pool surface, respectively. The dotted and dashed lines represent splash crown formation and Duez cavity formation, respectively, and the symbols indicated the cavity type, which are all shown in figure 2(b).

sphere and a quasistatic seal cavity forms in its wake (figure 3b,c,  $We = 7.9$ ). As  $We$  increases, the rim thins and grows taller due to its increasing upward velocity, which allows it to begin to climb the surface of the sphere, as seen in figure 3(a) at  $We = 109$ . The upward velocity and adherence of the rim to the sphere directly competes with the rate of sphere submergence. This causes the water to move up and around the top of the sphere faster as it descends below the original free-surface plane, resulting in less air entrainment and the formation of increasingly smaller cavities. Hence, the pinch-off time  $t_p$ , depth of the sphere at pinch-off  $h_b$ , and the pinch-off depth  $h_p$ , all decrease with increasing  $We$ , which can be seen qualitatively in figure 3 and quantitatively in figure 4. Once  $We \gtrsim 240$  (dotted line) the rim has formed into a splash crown that adheres to the sphere and has enough upward velocity to reach the top of the sphere by the time the top of the sphere has descended to the level of the undisturbed free surface ( $h_b = 1$  and  $h_p = 0$ , figure 4b,c), as seen at  $We = 269$  in figure 3(b,c). Hence, the formation of the splash crown (which adheres to the sphere) suppresses cavity formation and we will call the dotted lines in figures 2(a,b) and 3 the splash crown formation line. The convergence of the splash crown on the top of the sphere looks similar to convergence of the thin films on the top of a viscous drop impacting on a pool of low viscosity, as seen by Marston & Thoroddsen (2008).

As  $We$  increases above the splash crown formation line the splash crown climbs up the sphere surface faster, causing  $h_p$  to gradually rise above the free surface (figure 4c), and decreasing both  $t_p$  (figure 4a) and  $h_b$  (figure 4b). Around  $U_{cr}$ , a small asymmetric cavity forms with the splash crown quickly doming over the top (figure 3,  $We = 2696$ ). Once  $U_{cr}$  is reached, the splash crown has enough velocity to separate from the sphere and a large surface seal cavity forms (figure 3,  $We = 8081$ ). Hence, we see that cavity formation or suppression is governed by the formation and separation of the splash crown. Also, we find that cavity formation occurs in two regimes: at low enough  $We$  that a splash crown does not form, and at high enough impact velocity that the splash

## Water entry of spheres with various contact angles

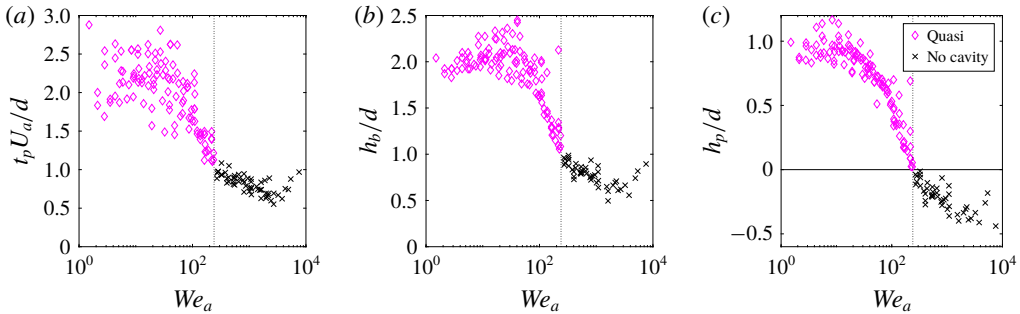


FIGURE 4. (a) The non-dimensional pinch-off time  $t_p$ , (b) depth of the bottom of the sphere at pinch-off  $h_b$  and (c) the pinch-off depth  $h_p$  scale with  $We_a$  for the quasistatic and no-cavity regimes for  $\theta = 86^\circ$  and  $101^\circ$  (same data as figure 2a,b). Figure 3(c) shows the same trends for  $h_b$  and  $h_p$  qualitatively, except that here the surface seal data is not shown as transition occurs at a constant velocity and hence the transition does not collapse with  $We_a$ . The dotted line represents the splash crown formation line. Note that the Weber number and dimensionless pinch-off time are defined using the average sphere velocity from initial impact to full submergence  $U_a$  ( $We_a = \rho U_a^2 d / \sigma$ ). This accounts for the continued acceleration of the sphere when it has not reached the terminal velocity in water by the time it impacts (e.g., an 18 mm sphere falling 3 mm). The legend in (c) applies to all three plots.

crown separates from the sphere. The boundaries of the no-cavity regime are defined by splash crown formation and what we will call Duez cavity formation (dotted and dashed lines in figures 2a,b and 3, respectively).

Surface seal is caused by the collapse of the splash crown. In the ideal cases typically depicted in the literature, the collapse of the crown, also known as dome over, causes a complete seal between the air in the cavity and the atmosphere (see supplementary movie 5). Figure 5 shows an event in which a complete seal does not occur during dome over. At  $t = 6.4$  ms, the splash crown has domed over and the air cavity behind the sphere begins to pull away from the free surface of the pool. At  $t = 8.0$ – $9.6$  ms, air continues to enter the cavity, as evidenced by the small conical structure that forms and connects the top of the cavity to the surface of the pool. The conical structure then collapses radially slightly below the surface, providing a complete seal ( $t = 11.2$  ms). These partial surface seal events could be caused by an asymmetric dome over of the splash crown, that leaves a small hole or by the formation of the thin-filmed bags observed by Marston *et al.* (2016) that pop, leaving holes in the crown. Partial surface seal occurs most commonly just above the critical velocity for cavity formation and at lower contact angles.

At the highest contact angle tested, when  $\theta = 141^\circ$  Duez *et al.* (2007) predict that cavities should form above a critical velocity of  $U_{cr} = (7/270)(\sigma/\mu)(\pi - \theta)^3 = 0.58$  m s $^{-1}$ . This velocity gives  $We < 240$  for all sphere diameters tested. Hence, the Duez cavity formation line lies below the splash crown formation line at all  $Bo$  tested and we would expect cavities to form at all impact velocities. This is indeed the case, as shown in figure 2(d). Comparing figure 2(d) to the data obtained by Aristoff & Bush (2009) for rough spheres with  $\theta = 120^\circ$  (shown in figure 2c) we see that the regime locations for the two coatings are very similar. Discrepancies in the cutoff between quasistatic seal and shallow or deep seal are possibly due to the lower atmospheric pressure in Logan, Utah (elevation of 1382 m) where our

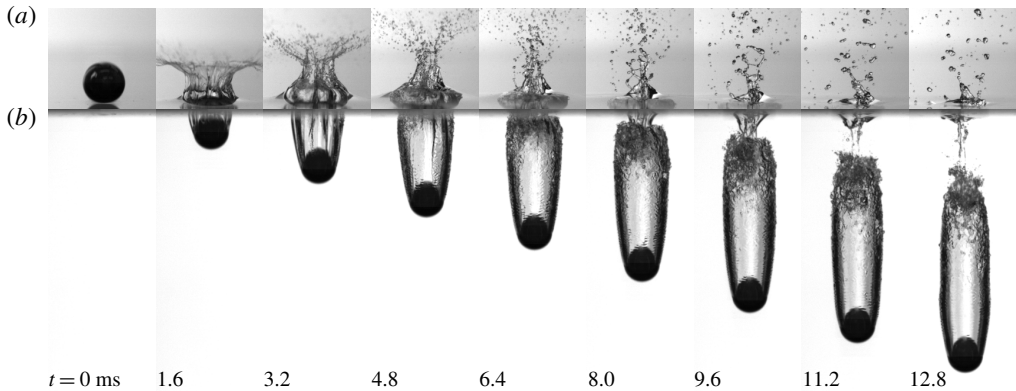


FIGURE 5. A sphere with  $d = 10$  mm and  $\theta = 101^\circ$  impacts the pool surface at  $U = 6.26$  m s<sup>-1</sup> forming a surface seal cavity with the above and below water views shown in (a,b) respectively. The splash crown does not always provide a complete seal of the cavity during dome over. Sometimes it mostly seals, but allows some air to continue to enter the cavity, as shown by the conical air pocket near the surface and above the main portion of the cavity at  $t = 9.6$  ms. The conical portion of the cavity then collapses radially ( $t = 11.2$ – $12.8$  ms). See supplementary movie 6.

experiments were performed and Cambridge, Massachusetts (elevation of 40 m) where the experiments of Aristoff & Bush (2009) were performed, with the lower pressure leading to less air entrainment, as shown by Gilbarg & Anderson (1948), persisting for larger  $We$ . Discrepancies could also be due to the difference in roughness or the difference in wetting angle, or all three effects combined.

Spheres rebound off the pool surface at the lowest  $Bo$  and  $We$  tested for all three contact angles. Figure 2 shows that transition from water entry to rebound occurs when  $We < 1$  and  $Bo < 0.5$ . In this parameter space, surface tension dominates over both inertial and gravitational forces and, hence, neither the sphere's inertia nor its weight cause it to enter the water surface. Figure 2 also shows that rebound is slightly dependent on the sphere's contact angle, with higher contact angles leading to rebound at higher  $Bo$  and  $We$ .

#### 4. New scaling to predict cavity regimes for various impacting bodies

When defining dimensionless numbers it is always difficult to pick the appropriate length and velocity scales to describe the physics of the problem. Historically in water entry research, the sphere diameter or radius has been chosen as the length scale and the initial impact velocity for the velocity scale (Truscott *et al.* 2014). As the cavity collapse is likely to be a function of the cavity characteristics, it could be insightful to redefine the appropriate dimensionless numbers using cavity length and velocity scales. We define the cavity Weber number as  $We_c = \rho U_c^2 d_c / \sigma$ , the cavity Bond number as  $Bo_c = \rho g d_c^2 / \sigma$  and the cavity Froude number as  $Fr_c = U_c^2 / g d_c$ , where  $d_c$  is the cavity diameter defined in § 2 as an averaged maximum diameter and  $U_c$  is the downward cavity velocity. We set  $U_c$  equal to the initial sphere impact velocity  $U_o$  as they are approximately the same over the time of cavity collapse. Plotting a regime diagram with the cavity scaling for  $\theta = 141^\circ$ , we see in figure 6 that  $Bo_c$  and  $We_c$  separate the cavity types for shallow, deep and surface seal (hollow symbols). Quasistatic seal



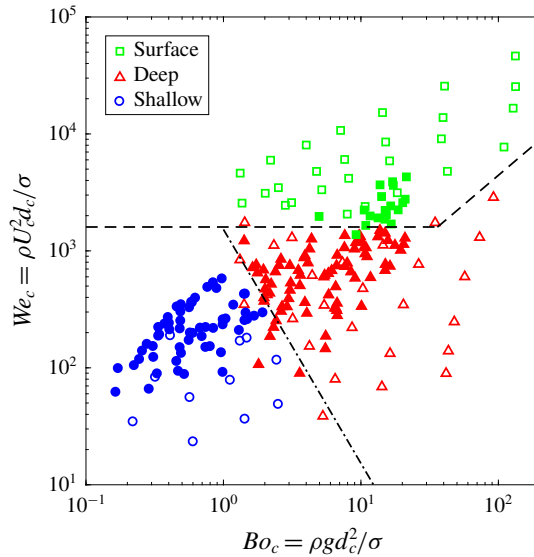


FIGURE 6. The cavity regimes can be predicted for various impacting bodies using the cavity diameter  $d_c$  and cavity velocity  $U_c$  to define  $Bo_c$  and  $We_c$ . The hollow symbols are for spheres (same as figure 2d) and the solid symbols are for multidroplet streams and jets. For spheres,  $U_c = U_o$ , and for multidroplet streams and jets,  $U_c$  is set equal to  $1/2U_{stream}$ . The dash-dotted line separating the shallow and deep seal regimes is found by equating the dimensionless pinch-off times for shallow and deep seal (figure 7). The dashed line dividing deep and surface seal is drawn by modifying the cutoffs found by Birkhoff & Isaacs (1951) and Aristoff & Bush (2009).

cavities are not included because they are not cylindrical, and they are specific to sphere entry, as discussed more in the next paragraph.

Speirs *et al.* (2018) investigated the water entry of multidroplet streams and jets and found that shallow, deep and surface seal cavities occur for liquid–liquid impact as well. Previous work had only shown shallow seal for multidroplet streams (Bouwhuis *et al.* 2016) and deep seal for jets (Oguz, Prosperetti & Lezzi 1992; Oguz, Prosperetti & Kolaini 1995; Zhu, Oguz & Prosperetti 2000; Qu *et al.* 2013). In that paper we predicted the cavity seal types for both multidroplet streams and jets on the same  $Bo$ – $We$  regime diagram (figure 6c of Speirs *et al.* (2018)) using a scaling based on the cavity diameter (figure 5 of Speirs *et al.* (2018)) and no alteration of the impact velocity. We can collapse those data onto the  $Bo_c$ – $We_c$  regime diagram for spheres, figure 6, using  $d_c$  and  $U_c$  to define  $Bo_c$  and  $We_c$ . (The regime diagram in figure 6c of Speirs *et al.* (2018) uses the stream velocity, jet diameter and a modified droplet diameter in the calculation of the Bond and Weber numbers.) The cavity velocity  $U_c$  is set equal to one half the impacting stream velocity, which is shown to be a good approximation for jets in multiple works (Oguz *et al.* 1992, 1995; Zhu *et al.* 2000; Qu *et al.* 2013; Speirs *et al.* 2018). Using this scaling, figure 6 shows that the regimes for all three water entry types (spheres, liquid jets and liquid multidroplet streams) can be predicted in the same  $Bo_c$ – $We_c$  parameter space. This scaling suggests that we can predict the pinch-off type of a cavity if we know its diameter and downward velocity, regardless of the type of impacting body used.

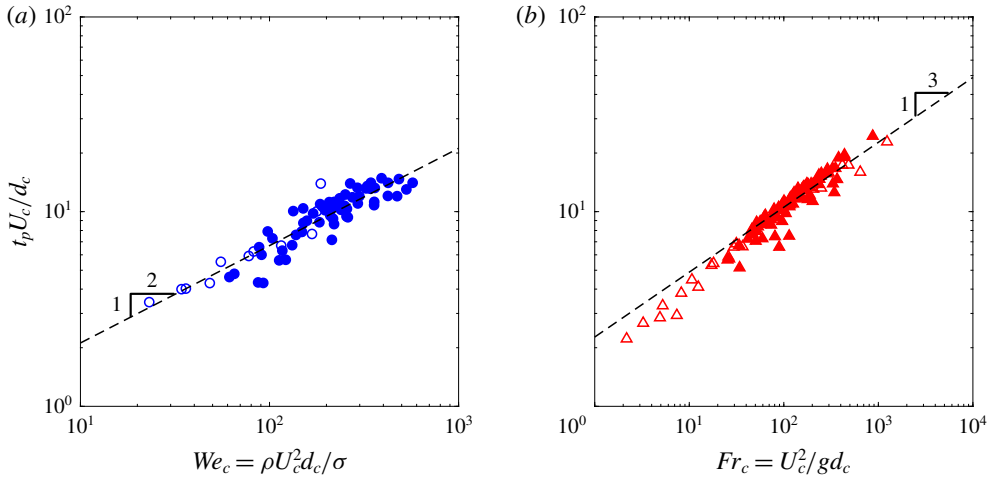


FIGURE 7. The non-dimensional cavity pinch-off time scales with  $We_c$  and  $Fr_c$  for (a) shallow and (b) deep seal for spheres with contact angle  $\theta = 141^\circ$  (hollow symbols) and multidroplet streams and jets (solid symbols). The dashed lines are fits to the data with powers forced to  $t_p U_c / d_c = 0.67 We_c^{1/2}$  for shallow seal and  $t_p U_c / d_c = 2.27 Fr_c^{1/3}$  for deep seal.

The cavity non-dimensional pinch-off times,  $t_p U_c / d_c$ , of the sphere, multidroplet stream and jet data can be predicted on the same plot for shallow and deep seal using  $We_c$  and  $Fr_c$ , respectively. Figure 7(a) shows that  $t_p U_c / d_c$  scales with  $We_c^{1/2}$  for shallow seal and figure 7(b) shows that  $t_p U_c / d_c$  scales with  $Fr_c^{1/3}$  for deep seal as also shown by Oguz *et al.* (1995), Lohse *et al.* (2004) and Duclaux *et al.* (2007). Equating these non-dimensional pinch-off times and rearranging gives the cutoff between the shallow and deep seal regimes, as shown by the dash-dotted line in figure 6 ( $We_c = 1, 525 Bo_c^{-2}$ ).

To predict the cutoff for surface seal we look at previous works. Aristoff & Bush (2009) used an empirical fit of  $We = 640$  to define the cutoff for surface seal at low  $Bo$  while at high  $Bo$  Birkhoff & Isaacs (1951) predicted the cutoff to occur at  $Fr = (1/12800)(\rho/\rho_a)^2$ , where  $\rho_a$  is the air density. We can use these results to find the surface seal cutoff in terms of  $We_c$  and  $Fr_c$ . At low  $Bo_c$ , the cutoff is  $We_c = 640(d_c/d)_{mean}$ , where  $(d_c/d)_{mean} \approx 2.5$  is the mean cavity to sphere diameter ratio for the deep and surface seal data just above and below the transition at low  $Bo_c$ . This leads to a transition at  $We_c = 1600$ . At high  $Bo_c$ , the cutoff is  $Fr_c = (1/12800)(\rho/\rho_a)^2(d/d_c)_{mean}$ , where  $(d/d_c)_{mean} \approx 1.6$  is the mean for the deep and surface seal data just above and below the transition at high  $Bo_c$ . This leads to a transition at  $Fr_c = 44$  or  $We_c = 44 Bo_c$ . These transitional lines are shown in figure 6 with the dashed line and appropriately divide the deep and surface seal regimes. It is interesting to note that the shallow, deep and surface seal transition lines intersect at  $Bo_c = 1$ , indicating that when surface tension dominates over gravitational forces, shallow seal will always occur instead of deep.

Seeing the importance of the cavity diameter in calculating  $Bo_c$  and  $We_c$ , we now scale  $d_c$  for each pinch-off type. Plotting the non-dimensional cavity diameter  $d_c/d$  against  $We$  we see in figure 8(a) that the cavity diameter for the shallow seal data is a function of  $We$  and can be predicted with a linear fit of  $d_c/d = 0.0074 We + 1$ , where

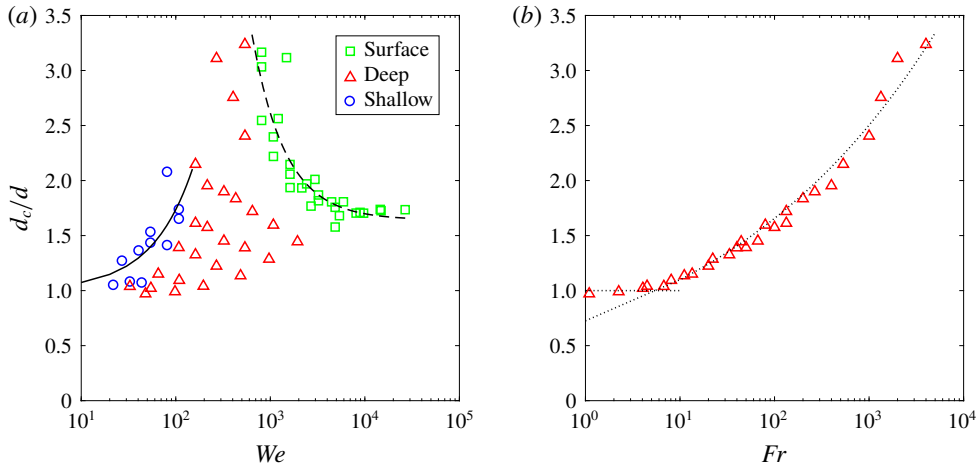


FIGURE 8. The cavity diameter for the impact of spheres with  $\theta = 141^\circ$  scales with  $We$  for shallow and surface seal (a) and  $Fr$  for deep seal (b). The solid and dashed lines in (a) are least square regressions with  $d_c/d = 0.0074We + 1$  for shallow seal and  $d_c/d = 4952We^{-1.24} + 1.64$  for surface seal. The curved dotted line in (b) is a fit for the deep seal data ( $d_c/d = 0.73Fr^{0.18}$ ), but for  $Fr < 7$  the cavity diameter approaches the sphere diameter,  $d_c/d = 1$ , marked by the horizontal dotted line.

the y-intercept is forced to equal one sphere diameter. We can also predict the cavity diameter for the surface seal data using  $We$  with the fit  $d_c/d = 4952We^{-1.24} + 1.64$ . As commonly seen, the deep seal data scales better with  $Fr$ , as shown in figure 8(b), and can be predicted by  $d_c/d = 0.73Fr^{0.18}$  for high  $Fr$ ; but below  $Fr \approx 7$  the ratio  $d_c/d$  asymptotes to one.

## 5. Conclusion

Cavity formation is dependent on the formation and behaviour of the splash crown. Three crown behaviours exist. (1) At low  $We$ , a slow-moving, thick rim forms around the sphere, which allows air to entrain in the wake of the sphere, forming small cavities. (2) At higher  $We$ , the crown thins, allowing it to adhere to the sphere, and gains velocity, allowing it to climb the surface and meet at the apex prior to full submergence to prevent cavity formation. (3) Once the critical velocity for cavity formation is reached, the splash crown separates from the sphere, forming the classical cavities discussed above and in previous works. The cutoffs between these behaviours are defined by splash crown formation, which is shown to be independent of contact angle for  $\theta = 86^\circ$  and  $\theta = 101^\circ$ , and Duez cavity formation, which is dependent on contact angle. For hydrophilic and slightly hydrophobic spheres, the inception of splash crown formation and adherence to the sphere decreases the cavity size, compared to higher contact angles, leading to quasistatic seal and small shallow seal cavities. When the contact angle is high enough ( $\theta \gtrsim 140^\circ$ ) or the sphere is rough (Zhao *et al.* 2014), cavities form at all impact velocities because the splash crown either does not form or it separates from the sphere. These cavity formation regimes are predicted by Aristoff & Bush (2009). When cavity formation is not inhibited by the splash, the pinch-off type can be predicted by the cavity diameter and downward cavity velocity regardless of the type of impacting body (e.g., sphere,

jet, or multidroplet stream). This forms a more complete picture, linking the impact of solids and liquids on liquid pools.

## Acknowledgements

N.B.S., T.T.T. and J.B. acknowledge funding from the Office of Naval Research, Navy Undersea Research Program (grant N0001414WX00811), monitored by Ms Maria Medeiros. J.B. acknowledges funding from the Naval Undersea Warfare Center In-House Laboratory Independent Research programme, monitored by Mr N. Dubois. N.B.S. and T.T.T. acknowledge funding from the Utah State University Research and Graduate Studies Development Grant Program.

## Supplementary movies

Supplementary movies are available at <https://doi.org/10.1017/jfm.2018.985>.

## References

- ARISTOFF, J. M. & BUSH, J. W. M. 2009 Water entry of small hydrophobic spheres. *J. Fluid Mech.* **619**, 45–78.
- ARISTOFF, J. M., TRUSCOTT, T. T., TECHET, A. H. & BUSH, J. W. M. 2010 The water entry of decelerating spheres. *Phys. Fluids* **22** (3), 032102.
- BIRKHOFF, G. & ISAACS, R. 1951 Transient cavities in air-water entry. Navord Report 1490. *Tech. Rep.*
- BOUWHUIS, W., HUANG, X., CHAN, C. U., FROMMHOLD, P. E., OHL, C.-D., LOHSE, D., SNOEIJER, J. H. & VAN DER MEER, D. 2016 Impact of a high-speed train of microdrops on a liquid pool. *J. Fluid Mech.* **792**, 850–868.
- DUCLAUX, V., CAILLÉ, F., DUEZ, C., YBERT, C., BOCQUET, L. & CLANET, C. 2007 Dynamics of transient cavities. *J. Fluid Mech.* **591**, 1–19.
- DUEZ, C., YBERT, C., CLANET, C. & BOCQUET, L. 2007 Making a splash with water repellency. *Nat. Phys.* **3** (3), 180–183.
- GILBARG, D. & ANDERSON, R. A. 1948 Influence of atmospheric pressure on the phenomena accompanying the entry of spheres into water. *J. Appl. Phys.* **19**, 127–139.
- HURD, R. C., BELDEN, J., JANDRON, M. A., FANNING, D. T., BOWER, A. F. & TRUSCOTT, T. T. 2017 Water entry of deformable spheres. *J. Fluid Mech.* **824**, 912–930.
- LOHSE, D., BERGMANN, R., MIKKELSEN, R., ZEILSTRA, C., VAN DER MEER, D., VERSLUIS, M., VAN DER WEELE, K., VAN DER HOEF, M. & KUIPERS, H. 2004 Impact on soft sand: void collapse and jet formation. *Phys. Rev. Lett.* **93**, 198003.
- MANSOOR, M. M., MARSTON, J. O., VAKARELSKI, I. U. & THORODDSEN, S. T. 2014 Water entry without surface seal: extended cavity formation. *J. Fluid Mech.* **743**, 295–326.
- MARSTON, J. O. & THORODDSEN, S. T. 2008 Apex jets from impacting drops. *J. Fluid Mech.* **614**, 293–302.
- MARSTON, J. O., TRUSCOTT, T. T., SPEIRS, N. B., MANSOOR, M. M. & THORODDSEN, S. T. 2016 Crown sealing and buckling instability during water entry of spheres. *J. Fluid Mech.* **794**, 506–529.
- MAY, A. 1951 Effect of surface condition of a sphere on its water-entry cavity. *J. Appl. Phys.* **22** (10), 1219–1222.
- OGUZ, H. N., PROSPERETTI, A. & KOLAINI, A. R. 1995 Air entrapment by a falling water mass. *J. Fluid Mech.* **294**, 181–207.
- OGUZ, H. N., PROSPERETTI, A. & LEZZI, A. M. 1992 Examples of air-entraining flows. *Phys. Fluids A* **4** (4), 649–651.
- QU, X., GOHARZADEH, A., KHEZZAR, L. & MOLKI, A. 2013 Experimental characterization of air-entrainment in a plunging jet. *Exp. Therm. Fluid Sci.* **44**, 51–61.

*Water entry of spheres with various contact angles*

- SPEIRS, N. B., PAN, Z., BELDEN, J. & TRUSCOTT, T. T. 2018 The water entry of multi-droplet streams and jets. *J. Fluid Mech.* **844**, 1084–1111.
- TRUSCOTT, T. T., EPPS, B. P. & BELDEN, J. 2014 Water entry of projectiles. *Annu. Rev. Fluid Mech.* **46** (1), 355–378.
- TRUSCOTT, T. T., EPPS, B. P. & TECHET, A. H. 2012 Unsteady forces on spheres during free-surface water entry. *J. Fluid Mech.* **704**, 173–210.
- TRUSCOTT, T. T. & TECHET, A. H. 2009a A spin on cavity formation during water entry of hydrophobic and hydrophilic spheres. *Phys. Fluids* **21** (12), 121703.
- TRUSCOTT, T. T. & TECHET, A. H. 2009b Water entry of spinning spheres. *J. Fluid Mech.* **625**, 135–165.
- ZHAO, M.-H., CHEN, X.-P. & WANG, Q. 2014 Wetting failure of hydrophilic surfaces promoted by surface roughness. *Sci. Rep.* **4**, 5376.
- ZHU, Y., OGUZ, H. N. & PROSPERETTI, A. 2000 On the mechanism of air entrainment by liquid jets at a free surface. *J. Fluid Mech.* **404**, 151–177.